nature neuroscience

The functional asymmetry of auditory cortex is reflected in the organization of local cortical circuits

Hysell V Oviedo[1], Ingrid Bureau[2], Karel Svoboda[3] & Anthony M Zador[1]

The primary auditory cortex (A1) is organized tonotopically, with neurons sensitive to high and low frequencies arranged in a rostro-caudal gradient. We used laser scanning photostimulation in acute slices to study the organization of local excitatory connections onto layers 2 and 3 (L2/3) of the mouse A1. Consistent with the organization of other cortical regions, synaptic inputs along the isofrequency axis (orthogonal to the tonotopic axis) arose predominantly within a column. By contrast, we found that local connections along the tonotopic axis differed from those along the isofrequency axis: some input pathways to L3 (but not L2) arose predominantly out-of-column. *In vivo* cell-attached recordings revealed differences between the sound-responsiveness of neurons in L2 and L3. Our results are consistent with the hypothesis that auditory cortical microcircuitry is specialized to the one-dimensional representation of frequency in the auditory cortex.

A widespread and appealing hypothesis is that all cortical areas (for example, visual and auditory) are wired according to the same general schema, regardless of what computation is performed in each area. According to this canonical model of cortical circuitry[1], information from the thalamus enters the cortex by way of thalamocortical synapses onto neurons in cortical layer 4 (L4), and these L4 neurons then transmit information to neurons in L2/3 and then to layer 5 (L5) (for example, refs. 2,3). This canonical circuit model represents the synthesis of several decades of careful neuroanatomy and neurophysiology probing the circuitry of visual cortex, the first area in which microcircuitry was examined in detail.

The introduction of laser scanning photostimulation (LSPS) has made it possible to examine the microcircuitry in other cortical areas with high efficiency. LSPS uses the photorelease of caged glutamate to map functional connections between a neuron and its presynaptic inputs *in vitro*[4,5]. This technique has revealed distinct patterns of functional connectivity in different cortical areas, including the whisker barrel somatosensory[3,6], motor[7] and auditory[8] cortices. These studies showed that although in broad strokes the canonical model of visual cortex may be valid in non-visual cortical areas, there are also important area-specific differences in local circuitry. Thus each cortical area may represent a variation on the canonical circuit, specialized for the implementation of the cortical computation that occurs within that area.

In the primary auditory cortex of all species studied so far, there is a characteristic map reflecting the tonotopic organization of sound frequency in the cochlea. In the mouse, as in many other species, high frequencies are represented in the rostral part of the cortex and low frequencies in the caudal[9]. This one-dimensional tonotopic axis can be considered the analog of two-dimensional space in the visual and somatosensory cortices, in that it reflects directly the organization of sensory receptors at the periphery. However, because the representation of sound frequency along the cochlea is intrinsically one-dimensional, the organization of auditory cortex along the axis orthogonal to the tonotopic cortical axis cannot immediately be inferred from the organization of the sensory periphery (but see ref. 10). The auditory cortex is thus functionally anisotropic: the functional organization along the tonotopic axis is qualitatively different from the organization orthogonal to the tonotopic axis. In this respect the auditory cortex differs from both the visual and somatosensory cortices, where the two-dimensional organization of the sensory periphery is reflected directly in the organization of the corresponding cortex. What is not known is how this functional anisotropy—that is, the spatial arrangement of tuned neurons—is reflected at the microcircuit level.

To determine how the functional anisotropy of auditory cortex observed *in vivo* is reflected in the local microcircuitry probed *in vitro*, we have used LSPS to compare the organization of mouse primary auditory cortex slices cut along the tonotopic axis with those cut perpendicular to that axis. Here we report that local inputs to L2/3 differ depending on whether or not the slice is cut to preserve information across frequencies. Furthermore, *in vivo* cell-attached recordings revealed differences between the sound-responsiveness of neurons in L2 and L3. Our results are consistent with the hypothesis that auditory cortical microcircuitry is specialized to the distinctive one-dimensional representation of frequency in the auditory cortex.

RESULTS

We first investigated the organization of synaptic inputs to L2/3 of mouse primary auditory cortex in a coronal slice cut to preserve isofrequency bands ('isofrequency slices'). We next examined the organization of inputs to L2/3 in a horizontal slice, which allowed us

[1]Cold Spring Harbor Laboratory, Cold Spring Harbor, New York, USA. [2]Institut National de la Santé et de la Recherche Médicale (INSERM), Unité 901, Institut de Neurobiologie de la Méditerranée, Marseille, France. [3]Janelia Farm Research Campus, Howard Hughes Medical Institute, Ashburn, Virginia, USA. Correspondence should be addressed to A.M.Z. (zador@cshl.edu).

Received 29 July; accepted 7 September; published online 17 October 2010; doi:10.1038/nn.2659

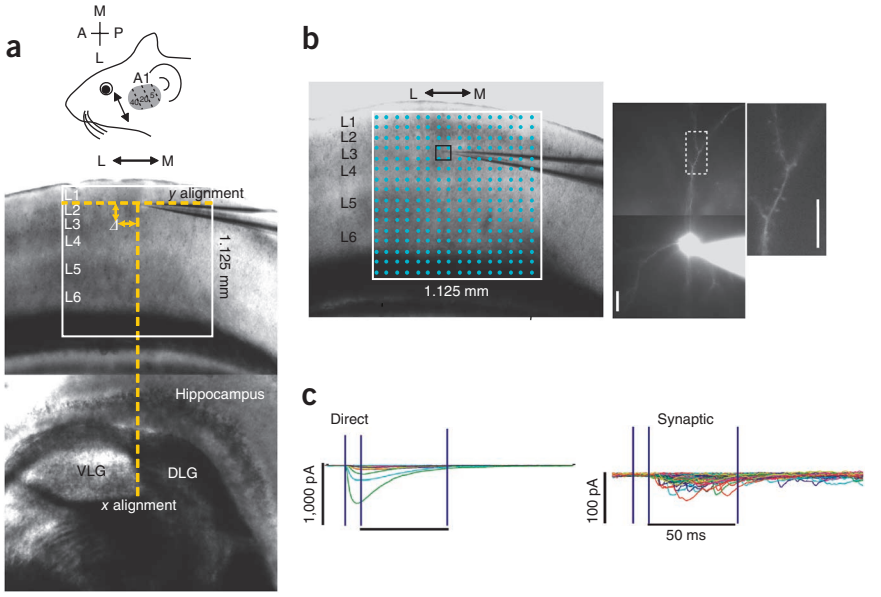

Figure 1 Auditory cortex LSPS experimental preparation. (**a**) Coronal brain slice (cut along the lateral (L) to medial (M) axis) containing the primary auditory cortex and underlying subcortical area, used for studying the organization along the isofrequency axis. The white box outlines the stimulus grid, and the dashed lines represent the landmarks used to align the grid from mouse to mouse. For each cell, we measured the distance of the soma from the L1–L2 border and the middle of the grid. (The ventral and dorsal divisions of the lateral geniculate nucleus (VLG and DLG, respectively) are labeled as landmarks.) A, anterior; P, posterior; 40, 20 and 5 (in kHz) represent the spatial organization of tone frequency tuning (tonotopy) in A1. (**b**) Left, stimulus grid showing the 16 × 16 points of uncaging. Right, picture of a patched cell filled with Alexa and magnification of a dendritic branch (scale bar, 15 µm). (**c**) Left, examples of direct responses—those evoked by the direct activation of receptors by uncaged glutamate in the neuron under study. Right, examples of synaptic responses—EPSCs elicited by triggering action potentials in neurons presynaptic to the neuron under study. Note difference in scale between left and right. The vertical lines through the traces mark the time window to detect direct responses (first two vertical lines) and synaptic events (second and third vertical lines).

to probe organization across different frequencies ('tonotopic slices'). Finally, we performed *in vivo* cell-attached recordings targeted at L2/3 neurons to explore whether the differences in local circuitry we observed *in vitro* lead to functional differences in stimulus-driven responses *in vivo*.

Organization of inputs to L2/3 along the isofrequency axis

We began by studying the input to neurons in L2/3 in a coronal slice that preserves isofrequency bands (**Fig. 1a**, top); that is, in a slice containing neurons that respond to similar frequencies[9]. The organization of the primary auditory cortex along this axis has recently been characterized in the rat[8], but to assess any species-specific differences in input pattern (as has been shown in the barrel cortex[6], for example) and to provide a baseline for the studies presented here, we repeated these experiments in the mouse.

We performed whole-cell recordings from excitatory neurons ($n = 26$) in L2/3 and isolated excitatory postsynaptic currents (EPSCs) by voltage-clamping near the inhibitory reversal potential (−70 mV). To characterize synaptic inputs, we added caged glutamate to the fluid bathing the slice and photoreleased at the focal spot of an ultraviolet laser beam (see Online Methods and **Fig. 1b**, left). Photorelease of caged glutamate near the patched neuron evoked a large, short-latency 'direct response' (**Fig. 1c**, left), mediated mainly by glutamate receptors near or on the soma, of sufficient magnitude to trigger one or a few action potentials under current clamp conditions. Photorelease of caged glutamate at other locations in the slice elicited either no response, or a 'synaptic response' (**Fig. 1c**, right). The synaptic responses, which are the focus of this study, result from action potentials in presynaptic neurons whose axons connect to the neuron from which we are recording. Direct responses can be distinguished from synaptic responses by their larger amplitudes and shorter latency (see Online Methods).

To facilitate comparison across experiments, we aligned the ultraviolet stimulation grid for all cells consistently, using landmarks in the slice (**Fig. 1a**, bottom; see Online Methods for details). To minimize differences arising from slice-to-slice variability in the alignment along the *x* axis of the grid with the landmarks, we present average population maps with all the somata aligned to the center of the map. We filled each neuron with a fluorescent marker (Alexa 594) to confirm that the dendritic tree was mostly contained within the slice, and to establish whether spines were present (**Fig. 1b**, right). All cells analyzed in this study were excitatory, as based on morphology and the presence of spines.

Representative synaptic input maps for neurons in L2 and L3 in isofrequency slices are shown in **Figure 2a** and **Figure 2b**, respectively. (See **Supplementary Fig. 1** for all input maps analyzed.) The pattern of input into L2/3 largely followed the columnar organization of the canonical cortical circuit. Averaging across slices (**Fig. 2c**), we found that the intralaminar connections from L2 and L3 provided the largest source of input, followed by L4 and L5, with only a small contribution from layer 6 (L6) (**Fig. 2d**, left).

To examine specific differences between inputs to L2 and L3 we examined the average input to each layer separately (**Fig. 2d**, right). Neurons in L2 and L3 were readily distinguished on the basis of previously described laminar boundaries[11] and our own experimental observations that (i) L2 appears as the densest cortical layer under infrared gradient contrast optics (average thickness of 100 µm; see **Fig. 3a**), and (ii) there are significant morphological differences between neurons in L2 and L3 (see below for examples, and ref. 6). L2 neurons had a non-classic pyramidal shape with their apical dendrites branching close to the cell body, whereas L3 neurons had a classic pyramidal shape. Quantitative comparison of the inputs to L2 ($n = 11$ neurons) and L3 ($n = 15$ neurons) revealed largely similar inputs to both layers, with the exception of significant input from deep layers to L2 but not to L3 (**Fig. 2d**, right). This input arose from the border between L5 and L6 and was not observed in the rat auditory cortex[8]. L3 had strong recurrent connections that are also largely absent in the rat. However, given the extensive lemniscal thalamocortical projections in L3 of the mouse[12], the prominent L3 to L3 connections we observed in the mouse may not represent a significant deviation from the classic L4 to L3 pathway.

Asymmetric inputs to L2/3 along the tonotopic axis

The laminar and columnar organization of synaptic inputs to L2/3 described so far were observed in a slice preparation that did not preserve the tonotopic map of the auditory cortex. To examine the

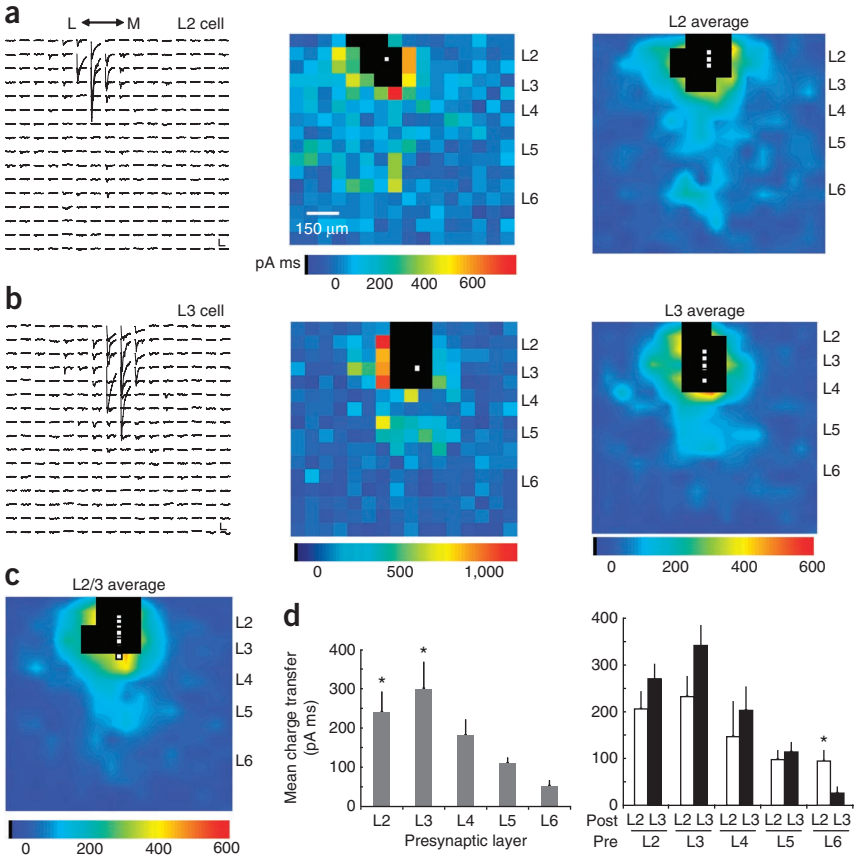

Figure 2 Synaptic input organization along the isofrequency axis. (**a**) Map of synaptic traces (left) used to generate the color map (middle) of a L2 neuron. Each trace on the left (and the corresponding pixel on the right) corresponds to a point on the uncaging grid (**Fig. 1b**). Pixels contaminated with a direct response are shown in black; for other pixels, the color indicates the charge transferred during the EPSC integration window defined in **Figure 1c**. The white square indicates the location of the soma. Right, interpolated average input map for all L2 neurons recorded ($n = 11$). Maps were realigned to place the somata on the center of the x axis of the map. Scale bars in **a** and **b**, 50 pA and 100 ms. (**b**) L3 single-cell trace map (left) and color map (middle), and interpolated population map (right) of all L3 neurons recorded ($n = 15$). (**c**) Interpolated map of all L2/3 neurons combined ($n = 26$). (**d**) Left, mean laminar input ($n = 26$) to L2/3 neurons (layers analyzed together). Local connections (within L2/3) provided most of the input for the population of L2 and L3 neurons recorded (*$P << 0.01$, one-way analysis of variance). Right, summary of the mean laminar input to L2 and L3 (layers analyzed separately) arising from all cortical layers. Pre, presynaptic layer; post, postsynaptic. *$P < 0.05$, presynaptic laminar input for which the difference between L2 and L3 was significant ($n = 26$, t-test). Data are presented as mean ± s.e.m. Scale bars in synaptic traces (**a**,**b**), 50 pA and 100 ms.

organization of synaptic inputs into L2/3 across the tonotopic axis (oriented anterior to posterior[9,13,14]), we conducted a new series of experiments using horizontal slices (**Fig. 3a**). These slices were prepared in the same orientation as the auditory thalamocortical slice preparation developed to optimize the input from the ventral division of the medial geniculate nucleus (MGBv) of the thalamus to A1 (ref. 12). We used the rostral tip of the hippocampus to align the stimulus grid along the x axis (**Fig. 3a**, bottom).

To confirm that our cortical recordings were indeed in A1, we performed two sets of control experiments using thalamocortical slices. First, we confirmed physiologically with thalamic LSPS experiments that there were direct synaptic inputs into L3 and L4 of the cortical area in which we performed all our subsequent cortical mapping experiments (**Supplementary Fig. 2**). Second, to confirm the anatomy, we made small injections of the retrograde tracer DiI into the putative A1 cortical area mapped (**Supplementary Fig. 3**). In all cases ($n = 6$) we found fibers labeled only in the MGBv, consistent with previous results[12]. These experiments confirmed that the cortical area mapped in horizontal slices was located within A1.

We investigated the functional organization of synaptic inputs within A1 across the tonotopic axis by recording from L2/3 excitatory cells ($n = 48$). We analyzed separately the inputs to neurons in L2/3 in tonotopic slices. Inputs to L2 ($n = 15$) in these slices showed a pattern similar to that found in L2 of the isofrequency slices. There was strong input from the border of L5–L6 and local connections (**Fig. 3b**, top and middle). Thus, the pattern of connectivity to L2 was the same along the tonotopic axis as across it.

By contrast, the pattern of inputs to L3 neurons ($n = 15$) in tonotopic slices differed from the pattern of inputs in isofrequency slices. Along the tonotopic axis, L6 input, which was largely absent in the isofrequency slices, emerged as an important source of input (**Fig. 3c–e**). Moreover, the L6 input was spatially shifted along the horizontal axis (**Fig. 3c**, middle): the L6 input did not arise mainly from within-column neurons located directly below the recorded neurons, but rather from more anterior sites of the primary auditory cortex, presumably corresponding to neurons tuned to higher frequencies.

To test whether this shift was somehow specific to the particular site from which we chose to record, we also recorded from pairs of L2/3 neurons separated by 250–300 µm in the same slice. We found that the connectivity was invariant to this translation along the tonotopic axis (**Supplementary Fig. 4**). We therefore grouped the data from the two clusters for further analysis. (See **Supplementary Figs. 5** and **6** for all input maps analyzed for tonotopic slices.) The average population map for L2 confirmed columnar input organization (**Fig. 3b**, bottom), and for L3 out-of-column L5/6 input (**Fig. 3c**, bottom) coupled with strong intralaminar input (**Fig. 3d**).

We characterized the asymmetry of input to L3 with several analyses. First, to quantify the horizontal shift on a cell-by-cell basis, we computed the horizontal distance between the soma of the recorded neuron and its deep L5 and L6 hotspot (d_{s-h}; see Online Methods for details). This analysis revealed a clear horizontal shift in the input to L3 (but not L2) along the tonotopic axis, but none along the isofrequency axis (**Fig. 4a**,**b**, top). Unlike L2 neurons, which received mainly columnar input, L3 cells received horizontally shifted inputs from as far as 400 µm from the soma ($P << 0.01$ for L2 versus L3, $n = 39$, t-test). Second, we calculated the average input arising from deep L5 and L6 from the average population maps (**Fig. 4a**,**b**, bottom). Consistent with the previous analysis of hotspots, this analysis revealed that inputs from deep L5 and L6 to L3 were shifted anteriorly with

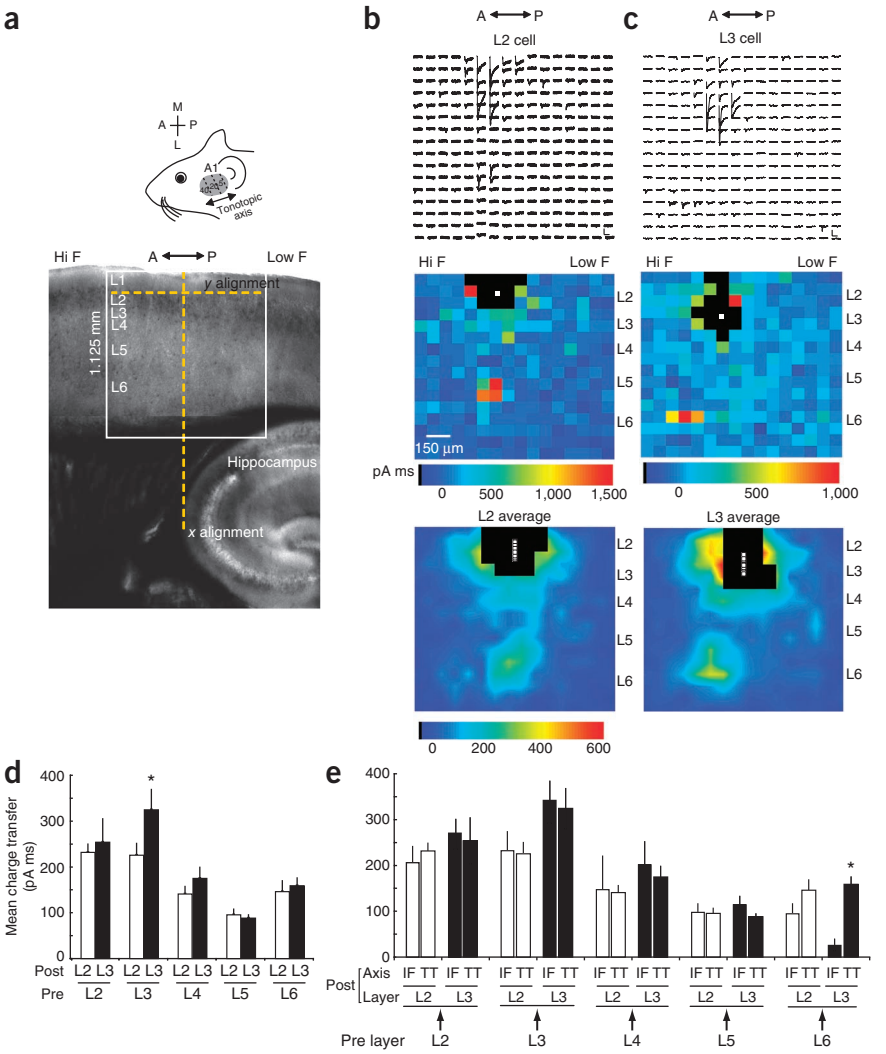

Figure 3 Synaptic input organization along the tonotopic axis. (**a**) Horizontal slices used to capture the anterior-posterior (A↔P) representation of tonotopy in auditory cortex. Image of a horizontal slice depicts the anatomical landmarks used to align the stimulation grid (white box). The anterior (left) side of the slice corresponds to the putative high frequency (Hi F) portion of A1 and the posterior (right) side to putative low frequencies (Low F). M, medial; L, lateral. (**b**) Trace map of synaptic input map to a L2 neuron (top) and its color map (middle). Interpolated population map of all L2 neurons recorded (bottom, $n = 15$). (**c**) L3 single-cell trace map (top) and color map (middle), and interpolated population map (bottom) of all L3 neurons recorded ($n = 15$). (**d**) Summary of the mean laminar input to L2 and L3 arising from all cortical layers. Asterisk indicates laminar input where the difference in synaptic input between L2 and L3 was significantly different ($P < 0.05$, $n = 30$, t-test). (**e**) Grand summary and comparison of the mean laminar input to L2/3 along the isofrequency (IF) and tonotopic (TT) axes. Asterisk indicates laminar input where the difference in synaptic input between the tonotopic and isofrequency axes was significantly different ($P << 0.01$, t-test). Data are presented as mean ± s.e.m. Scale bars in synaptic traces (**b**,**c**) 50 pA and 100 ms.

respect to L2 in tonotopic (**Fig. 4a**, bottom) but not isofrequency (**Fig. 4b**, bottom) slices. Because there is an anterior-posterior map of frequency in the primary auditory cortex, our results suggest that the input to L3 arises from out-of-column neurons in L6 tuned to higher frequencies.

Laminar input analysis showed that L3 contributed significantly more input to itself than to L2 in tonotopic slices (**Fig. 3d**). To determine whether this relative increase in L3 intralaminar input was due to an asymmetry in the connectivity within L3, we compared the intralaminar input within L3 (that is, the L3 to L3 input) arising from the higher frequency side to that arising from the lower frequency side. We found that the average L3 input from the higher frequency side was significantly stronger than from the lower frequency side in the tonotopic slices (**Fig. 4c**, left; $P < 0.05$, $n = 23$, t-test), but no such intralaminar input asymmetry was found in the isofrequency slices (**Fig. 4c**, right, $P = 0.85$, $n = 15$, t-test). Thus in addition to the bias in high frequency inputs from L6, there was also a tendency for local recurrent connections to arise from L3 neurons positioned at higher frequencies along the tonotopic axis. Taken together, these columnar and laminar differences of synaptic input into L3 across axes of stimulus representation suggest that L3 neurons receive disproportionately more input from neurons tuned to higher frequencies.

Shared input among nearby neurons

LSPS scanning showed that neurons in L2 and L3 received a large proportion of their input from nearby neurons in the same layer. Along the tonotopic axis, L2 and L3 received 45% of their input from local (L2 and L3) connections (**Fig. 3d**). Along the isofrequency axis, the proportion of local input was even higher: L2 received 54% and L3 60% from local connections (**Fig. 2d**, right). The contribution of intralaminar input to L2/3 in auditory cortex was higher than comparable values estimated using LSPS in visual (26%; ref. 2) and barrel (36% for L2 and 19% for L3; ref. 6) cortices. These values probably represent an underestimate of the contribution of local inputs because with LSPS very local (<100 µm) inputs are mixed with direct responses and thus are not included (see, for example, ref. 15).

Given that nearby neurons are highly interconnected, we wondered about the extent to which nearby neurons receive similar input. If the pattern of synaptic inputs to nearby neurons were very similar, this would support the idea that nearby neurons are performing similar—perhaps redundant—computations. To assess the similarity of inputs, we compared synaptic maps recorded from two or more neurons within a single slice. We quantified similarity by computing the correlation between pairs of average maps. A correlation of unity means that the input maps of two neurons are identical, whereas a correlation of zero means that the input to two neurons is independent. In practice, the maximum observable correlation is limited by noise, which can be estimated by computing the correlation of maps from a single neuron to itself. This procedure provided an average upper bound of approximately 0.75, similar to that reported in the barrel cortex[3].

The pairwise map correlation as a function of intersomatic distance is shown in **Figure 5**. For both tonotopic and isofrequency slices, the correlation was largest for neurons closest together and declined with

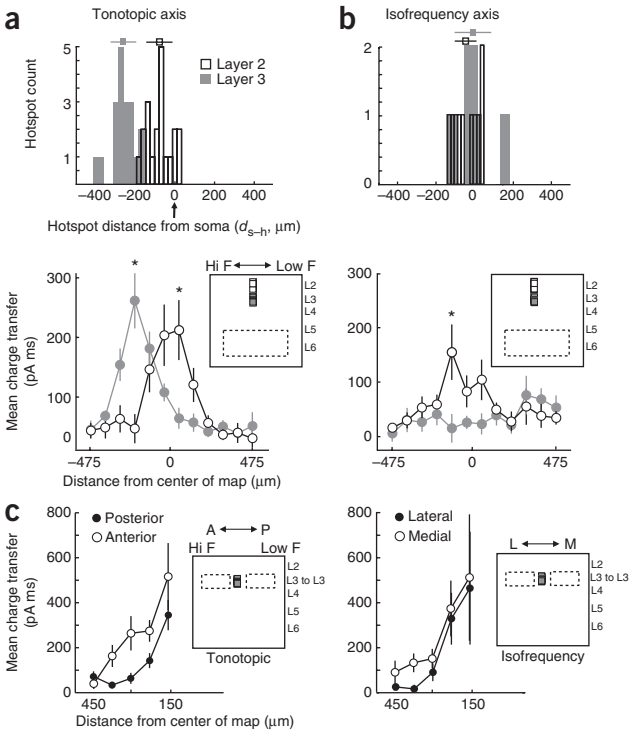

Figure 4 Along tonotopic but not isofrequency axis, inputs to L3 arise asymmetrically out-of-column. (**a**,**b**) L5/6 input to L3, but not L2, arose out-of-column preferentially from putative high-frequency (Hi F) neurons in tonotopic slices. Top panels show the distribution of the horizontal distances between the soma and its hotspot (d_{s-h}) of presynaptic input along the tonotopic ($n = 39$) and isofrequency ($n = 22$) axes for each L2 and L3 neuron. The square points show the mean (± s.e.m.) of the L2 and L3 distributions. Bottom panels show columnar average of L5/6 input. Asterisks indicate columns where input to L2 was significantly different from input to L3. The insets show the uncaging grids and the relative positions of the cortical area where inputs were averaged (dashed rectangles). (**c**) Local L3 input to L3 arose preferentially from putative high-frequency neurons in tonotopic slices. Relative contribution of local input (within L3) arising from the anterior and posterior (putative higher and lower frequency, respectively) input sites of the L3 cells mapped in the tonotopic slice. The plots show the mean charge transfer along columns. Input arising from the higher-frequency sites was greater than from lower frequency sites in the tonotopic slice (left), but not the isofrequency (right). Inputs arising from posterior and medial sites were reflected on the *x* axis for display purposes. Insets show the uncaging grid and the relative position of the cortical area where inputs were averaged (dashed rectangles to the left and right of L3 somata). Data are presented as mean ± s.e.m.

distance. The mean correlation between the nearest (<100 µm) pairs was 0.30 ± 0.02 and 0.34 ± 0.04 for the tonotopic and isofrequency slices, respectively, which was higher than that between more distant (>100 µm) pairs (0.2 ± 0.04 and 0.18 ± 0.04 for the tonotopic and isofrequency slices). To quantify the decrease in correlation with distance, we fitted the data with a simple exponential $c = 0.37e^{-x/159}$, where x is the intersomatic distance (in micrometers). Thus nearby neurons are not very correlated, and the correlation falls off rapidly, with a space constant of about 159 µm.

Differences in L2 and L3 response properties and projections

The differences we observed between L2 and L3 input patterns *in vitro* suggested that neurons in these layers might have functionally distinct responses to sounds (**Fig. 6**). To test this hypothesis, we used *in vivo* cell-attached methods[16] to compare tuning curves (100 and 500 ms pure tones, five octaves, four intensities) of neurons in L2/3. After each recording, we electroporated each neuron with biocytin for later histological analysis[17,18]. We recovered the morphology of 20 presumed (on the basis of the presence of spines) excitatory neurons with either a non-classic pyramidal shape ($n = 10$, found exclusively in L2, similar to mouse barrel cortex[6]; **Fig. 6a**, left) or classic pyramidal neurons ($n = 10$, found in L3, **Fig. 6b**, right). Based on their anatomical position, all cells recovered were within primary auditory cortex (**Fig. 6d**).

Tuning curves in L2 and L3 were clearly different (**Fig. 6a**,**b**). Pure tones increased the firing rate of L2 cells above background significantly more than it increased the firing rate of L3 cells ($P << 0.01$, $n = 20$, t-test; **Fig. 6c**). L2 neurons were more responsive, and they tended to be tuned to stimulus frequency in an intensity-dependent manner: tuning width (that is, the range of frequencies that elicited a response) increased with tone intensity (**Fig. 6a**, right). We did not recover any L3 neurons with clear frequency tuning; most showed little or no tone-evoked response (**Fig. 6b**, left). Responses to other stimuli, such as white noise, were also different (**Supplementary Fig. 7**).

Finally, we examined whether L2 and L3 also differed in their long-range projections. To test for differences, we chose the interhemispheric pathway between the auditory cortices. We injected the retrograde tracer cholera toxin in the right auditory cortex to reveal projections arising from the left auditory cortex (the hemisphere characterized in this study). The laminar pattern of interhemispheric projections revealed another difference between L2 and L3: L3 projected to the contralateral auditory cortex, whereas L2 did not (**Fig. 6e**; four out of four mice). Thus, the differences in local circuitry between L2 and L3 along the tonotopic axis are associated with differences in both long-range connectivity and sound-evoked responses *in vivo*, suggesting that these neuronal populations may be have different functions.

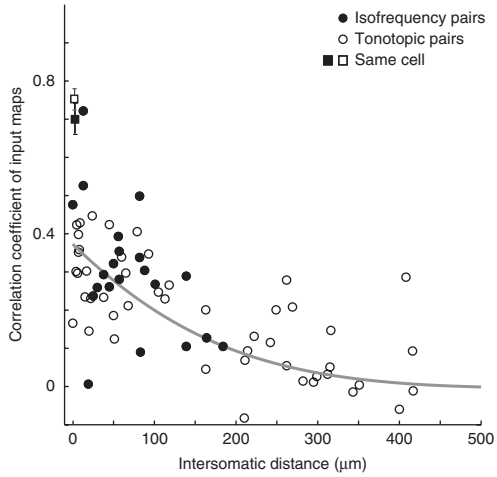

Figure 5 Synaptic input correlation between pairs of auditory cortical neurons. Plot shows the relationship between the correlations of input maps in pairs of cells in the same slice as a function of their intersomatic horizontal distance. We compared population correlation along the tonotopic and isofrequency axes. The gray line is the exponential fit ($0.37e^{-x/159}$). Square points showing the correlation of maps obtained for the same cell represent the theoretical upper limit of correlation given the experimental variability.

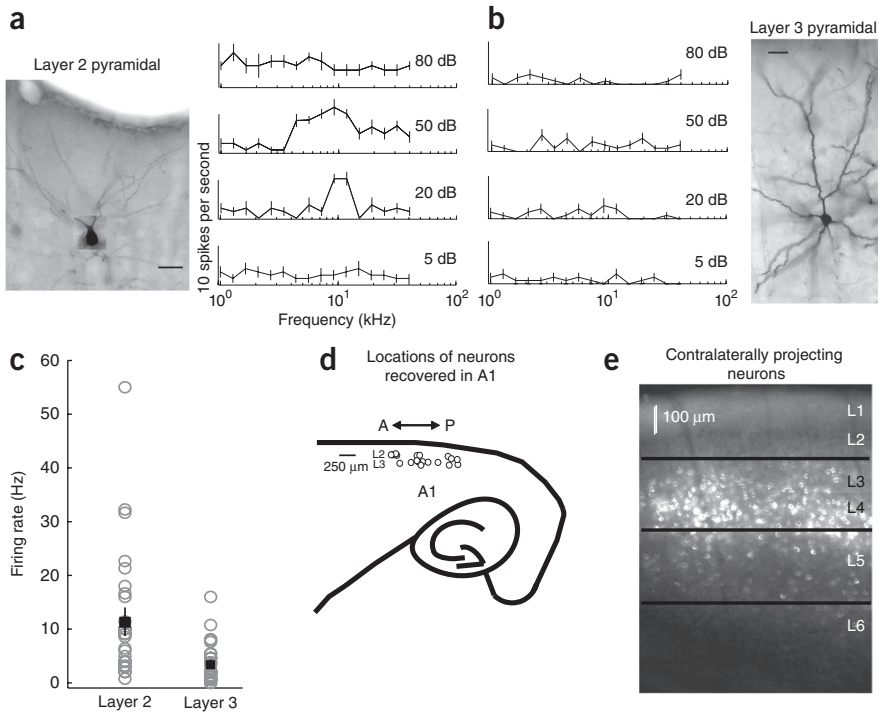

Figure 6 L3 neurons are less responsive to simple auditory stimuli than L2 neurons. (**a**) Frequency-response plot (right) for a L2 neuron (left) assessed using cell-attached recording. (**b**) Frequency-response plot (left) for a L3 neuron (right) assessed using cell-attached recording. Scale bars in **a** and **b**, 25 µm. (**c**) Summary of the differences in evoked firing rate between the L2 and L3 neurons recovered ($n = 20$). For each intensity, we found the octave bin with the maximum firing rate in the 150 ms post-stimulus epoch; we then averaged over the maximum for intensities 20, 50 and 80. The difference in firing rates was insensitive to outliers (for example, removing the three highest firing rates from each group increased significance from $P < 10^{-4}$ to $P < 10^{-5}$, $n = 20$, *t*-test). (**d**) Locations of neurons characterized in **c**. (**e**) Labeling in the left auditory cortex after injection of a retrograde tracer (cholera toxin) into the right auditory cortex, showing that L3 but not L2 neurons project to the contralateral auditory cortex. Data are presented as mean ± s.e.m.

DISCUSSION

We have used LSPS to study the local inputs to L2 and L3 in auditory cortex. Our main findings are that (i) the local input to L3 is anisotropic (that is, it is different along and across the tonotopic axis), with out-of-column input to L3 arising preferentially from higher frequencies, particularly from L3 and L6; (ii) nearby neurons share only modest input, and the amount of shared input decreases rapidly (space constant λ = 159 µm); and (iii) these differences in local circuitry are associated with functional differences in sound responsiveness.

Anisotropy of columnar structure in auditory cortex

The map of acoustic space in the auditory cortex is functionally anisotropic: there is a low-to-high frequency organization of neurons along the tonotopic axis that is absent along the orthogonal isofrequency axis. Our most unexpected finding was that this anisotropy was reflected in the local circuitry of inputs to L3, manifested as a difference between the local circuitry preserved within tonotopic and isofrequency slices. Specifically, in tonotopic slices, L3 neurons preferentially received inputs from out-of-column neurons in L6. Furthermore, the input from L6 was asymmetric, arising preferentially from anterior parts of the auditory cortex—corresponding to regions of the tonotopic map tuned to higher frequencies. This anisotropy in connectivity was not a general property of horizontal slices (for example, it was not present in nearby somatosensory areas; **Supplementary Fig. 8**) but seems to be a specific reflection of the unusually anisotropic auditory cortical map.

The high-frequency bias in tonotopic slices was most marked in L3 inputs from L6 and L3. The lateral distance of these shifted L6 inputs ranged from 200 to 400 µm (**Fig. 4a**). Given the size of the mouse auditory cortex (just over 1 mm along the horizontal plane covering six octaves[9]), the L3 cells receiving spectrally shifted input from L6 neurons could be integrating across at least one to three octaves. The bias towards high-frequency in the L3 to L3 input was comparably large.

Anisotropic organization along the tonotopic axis is not unique to the mouse. Differences in the connectivity between the tonotopic and isofrequency axes have previously been reported in both the rabbit[19] and the cat[20]. Although anisotropic organization was not previously reported in a study of coronal (isofrequency) rat primary auditory cortex slices[8], we observed in the rat clear evidence of anisotropy in horizontal (tonotopic) slices (**Supplementary Fig. 9**). This anisotropic organization may thus be a universal feature of auditory cortex across species.

L2 and L3 are distinct in auditory cortex

In many areas of cortex, no distinction is made between layers 2 and 3: L2/3 is treated as a single homogenous functional unit. Our results, however, indicated that in the auditory cortex, neurons in these two laminae were distinct with respect to morphology, connectivity and function. Morphologically, L2 and L3 pyramidal cells differed: L3 neurons had a classic pyramidal shape, whereas L2 cells lacked an elongated apical shaft and instead had dendrites that arborized parallel to the slice. At the level of local connectivity, the pattern of intracortical synaptic input was also distinct between these layers, especially along the tonotopic axis: L2 received columnar input, whereas L3 received out-of-column input. We also found that neurons in L3 but not in L2 projected to the contralateral cortex, as observed in the auditory cortex of the cat and rat[21–23].

Finally, neurons in the two layers differed functionally with respect to their responsiveness to simple auditory stimuli such as pure tones and white noise. L2 cells were more responsive and showed well-defined frequency tuning to pure tones, whereas L3 cells were largely unresponsive. This difference in responsiveness is consistent with recent results, using photostimulation-assisted identification of neuronal populations (PINP), showing that contralaterally projecting L3 neurons (functionally tagged with channelrhodopsin-2) are not responsive to simple auditory stimuli[23]. These observations suggest that L2 and L3 may be functionally distinct.

Although L2 and L3 appear functionally distinct in A1, the anatomical and functional boundary between L3 and L4 is less clear in A1 than in other sensory cortices. L4 in A1 lacks the characteristic spiny stellate cells found in other sensory regions[24] and sends projections to contralateral A1 (**Fig. 6e** and ref. 22.). L3 and L4 in A1 are very similar in several other respects: both layers receive equally strong

thalamic input (as measured by current source density[12]) and show equally strong cytochrome oxidase staining in the mouse[11], a feature that is classically used to identify L4 in other regions.

Weak local connectivity in auditory cortex

To what extent do nearby neurons in the cortex form a functional unit? In the primary visual cortex of cats and primates, neurons are functionally organized into orientation columns, defined by their shared preference for lines with a specific orientation in the visual field[25]. Columnar organization has since been described in many other cortical areas. A powerful form of columnar organization is found in the rodent whisker system[26], in which neurons within a cortical barrel encode activity of a single whisker and show strong local interconnectivity.

Strong columnar organization is not, however, universal across species and cortical areas. For example, the rodent visual cortex is not organized into orientation columns[27–29]; this is as predicted by theoretical considerations of wire length[30]. These differences in the extent of columnar organization, as measured by the similarity of sensory responsiveness of nearby neurons *in vivo*, are reflected in the local organization of connections *in vitro*. For example, unconnected nearby neurons in L2/3 of the rat visual cortex share little excitatory input from lower layers, consistent with a model in which there are two or more interdigitated "subnetworks"[31].

Although there is some degree of gross tonotopy in the rodent auditory cortex, neurons do not seem to be organized into functional columns: nearby neurons can respond quite differently to the same stimulus[32–34]. These differences in response properties reflect an increase in coding independence from the inferior colliculus[35]. Consistent with this *in vivo* organization, we found that the synaptic inputs to nearby neurons in L2 and L3 were quite different *in vitro*. Even for neurons closer than 100 µm, the pair-wise correlation of their input maps was 0.3, less than half of what is observed in the rat within a barrel—consistent with the much stronger columnar organization within barrels—and comparable to that observed in the septa (the regions between barrels[3]). Thus the weak tonotopic spatial organization found *in vivo* seems to be reflected in weak local connectivity.

Functional implications

Our main finding was that the organization of inputs onto L3 in primary auditory cortex differed along and orthogonal to the tonotopic axis. Although this anisotropy is, as far as is known, unique to the auditory cortex, it is consistent with the general principle that the organization of sensory maps reflects the statistics of sensory inputs. Just as the maps of space in the visual and barrel cortices mirror the organization of inputs at the retina and whiskers, respectively, the anisotropic organization of the auditory cortex reflects the one-dimensional organization of frequencies in the cochlea.

Perhaps the most unexpected observation was that the local circuits within A1 were not only anisotropic, but also asymmetric. In the tonotopic axis these connections could arise up to 400 µm from the L3 neurons we mapped (**Fig. 4a**), consistent with integration over at least three octaves[9]. Our data suggest that the L6 to L3 pathway may also serve to relay spectrally distant input from up to 400 µm away. Notably, the intralaminar and L6 pathways were not mutually exclusive; we routinely found L3 neurons that received input from both (**Supplementary Figs. 5** and **6**).

Neural circuits in A1 are involved in the processing of spectrally complex sounds, including vocalizations, which requires integration over many frequencies[36–38]. Our data support a model for auditory cortex[39,40], developed in part by analogy with the visual system[41,42], in which intralaminar horizontal connections within L3 mediate this spectral integration. In addition, our data suggest that an out-of-column L6 pathway, possibly unique to auditory cortex, may also contribute to this spectral integration. By combining LSPS and other *in vitro* approaches with new optogenetic[23,43], imaging[32,33] and other technologies, we are now positioned to understand how *in vivo* sound responsiveness arises from the underlying circuitry of the auditory cortex.

METHODS

Methods and any associated references are available in the online version of the paper at http://www.nature.com/natureneuroscience/.

Note: Supplementary information is available on the Nature Neuroscience website.

ACKNOWLEDGMENTS

We thank B. Burbach for invaluable technical help, S. Joshi for invaluable input on juxtacellular labeling, N. Gray, G. Otazu and T. Hackett for discussions, and W. Bair (Department of Physiology, Anatomy and Genetics, University of Oxford) for spike detection software. This work was supported by grants from the US National Institutes of Health, the Patterson Foundation (H.V.O.) the Swartz Foundation and Autism Speaks.

AUTHOR CONTRIBUTIONS

H.V.O. and A.M.Z. conceived the experiments, analyzed the data and wrote the paper. H.V.O. performed all the experiments. I.B. and K.S. provided expert advice and LSPS experimental set-up.

COMPETING FINANCIAL INTERESTS

The authors declare no competing financial interests.

Published online at http://www.nature.com/natureneuroscience/.
Reprints and permissions information is available online at http://npg.nature.com/reprintsandpermissions/.

1. Douglas, R.J. & Martin, K.A. Neuronal circuits of the neocortex. *Annu. Rev. Neurosci.* **27**, 419–451 (2004).
2. Dantzker, J.L. & Callaway, E.M. Laminar sources of synaptic input to cortical inhibitory interneurons and pyramidal neurons. *Nat. Neurosci.* **3**, 701–707 (2000).
3. Shepherd, G.M. & Svoboda, K. Laminar and columnar organization of ascending excitatory projections to layer 2/3 pyramidal neurons in rat barrel cortex. *J. Neurosci.* **25**, 5670–5679 (2005).
4. Callaway, E.M. & Katz, L.C. Photostimulation using caged glutamate reveals functional circuitry in living brain slices. *Proc. Natl. Acad. Sci. USA* **90**, 7661–7665 (1993).
5. Shepherd, G.M., Pologruto, T.A. & Svoboda, K. Circuit analysis of experience-dependent plasticity in the developing rat barrel cortex. *Neuron* **38**, 277–289 (2003).
6. Bureau, I., von Saint Paul, F. & Svoboda, K. Interdigitated paralemniscal and lemniscal pathways in the mouse barrel cortex. *PLoS Biol.* **4**, e382 (2006).
7. Weiler, N., Wood, L., Yu, J., Solla, S.A. & Shepherd, G.M. Top-down laminar organization of the excitatory network in motor cortex. *Nat. Neurosci.* **11**, 360–366 (2008).
8. Barbour, D.L. & Callaway, E.M. Excitatory local connections of superficial neurons in rat auditory cortex. *J. Neurosci.* **28**, 11174–11185 (2008).
9. Stiebler, I., Neulist, R., Fichtel, I. & Ehret, G. The auditory cortex of the house mouse: left-right differences, tonotopic organization and quantitative analysis of frequency representation. *J. Comp. Physiol. [A]* **181**, 559–571 (1997).
10. Read, H.L., Winer, J.A. & Schreiner, C.E. Functional architecture of auditory cortex. *Curr. Opin. Neurobiol.* **12**, 433–440 (2002).
11. Anderson, L.A., Christianson, G.B. & Linden, J.F. Mouse auditory cortex differs from visual and somatosensory cortices in the laminar distribution of cytochrome oxidase and acetylcholinesterase. *Brain Res.* **1252**, 130–142 (2009).
12. Cruikshank, S.J., Rose, H.J. & Metherate, R. Auditory thalamocortical synaptic transmission *in vitro*. *J. Neurophysiol.* **87**, 361–384 (2002).
13. Kimura, A., Donishi, T., Sakoda, T., Hazama, M. & Tamai, Y. Auditory thalamic nuclei projections to the temporal cortex in the rat. *Neuroscience* **117**, 1003–1016 (2003).
14. Linden, J.F., Liu, R.C., Sahani, M., Schreiner, C.E. & Merzenich, M.M. Spectrotemporal structure of receptive fields in areas AI and AAF of mouse auditory cortex. *J. Neurophysiol.* **90**, 2660–2675 (2003).
15. Lefort, S., Tomm, C., Floyd Sarria, J.C. & Petersen, C.C. The excitatory neuronal network of the C2 barrel column in mouse primary somatosensory cortex. *Neuron* **61**, 301–316 (2009).

16. DeWeese, M.R., Wehr, M. & Zador, A.M. Binary spiking in auditory cortex. *J. Neurosci.* **23**, 7940–7949 (2003).
17. Pinault, D. A novel single-cell staining procedure performed *in vivo* under electrophysiological control: morpho-functional features of juxtacellularly labeled thalamic cells and other central neurons with biocytin or Neurobiotin. *J. Neurosci. Methods* **65**, 113–136 (1996).
18. Joshi, S. & Hawken, M.J. Loose-patch-juxtacellular recording *in vivo*—a method for functional characterization and labeling of neurons in macaque V1. *J. Neurosci. Methods* **156**, 37–49 (2006).
19. Velenovsky, D.S., Cetas, J.S., Price, R.O., Sinex, D.G. & McMullen, N.T. Functional subregions in primary auditory cortex defined by thalamocortical terminal arbors: an electrophysiological and anterograde labeling study. *J. Neurosci.* **23**, 308–316 (2003).
20. Matsubara, J.A. & Phillips, D.P. Intracortical connections and their physiological correlates in the primary auditory cortex (AI) of the cat. *J. Comp. Neurol.* **268**, 38–48 (1988).
21. Imig, T.J. & Brugge, J.F. Sources and terminations of callosal axons related to binaural and frequency maps in primary auditory cortex of the cat. *J. Comp. Neurol.* **182**, 637–660 (1978).
22. Games, K.D. & Winer, J.A. Layer V in rat auditory cortex: projections to the inferior colliculus and contralateral cortex. *Hear. Res.* **34**, 1–25 (1988).
23. Lima, S.Q., Hromádka, T., Znamenskiy, P. & Zador, A.M. PINP: a new method of tagging neuronal populations for identification during in vivo electrophysiological recording. *PLoS ONE* **4**, e6099 (2009).
24. Smith, P.H. & Populin, L.C. Fundamental differences between the thalamocortical recipient layers of the cat auditory and visual cortices. *J. Comp. Neurol.* **436**, 508–519 (2001).
25. Hubel, D.H. & Wiesel, T.N. Receptive fields, binocular interaction and functional architecture in the cat's visual cortex. *J. Physiol. (Lond.)* **160**, 106–154 (1962).
26. Armstrong-James, M., Fox, K. & Das-Gupta, A. Flow of excitation within rat barrel cortex on striking a single vibrissa. *J. Neurophysiol.* **68**, 1345–1358 (1992).
27. Van Hooser, S.D., Heimel, J.A., Chung, S., Nelson, S.B. & Toth, L.J. Orientation selectivity without orientation maps in visual cortex of a highly visual mammal. *J. Neurosci.* **25**, 19–28 (2005).
28. Van Hooser, S.D., Heimel, J.A., Chung, S. & Nelson, S.B. Lack of patchy horizontal connectivity in primary visual cortex of a mammal without orientation maps. *J. Neurosci.* **26**, 7680–7692 (2006).
29. Ohki, K., Chung, S., Ch'ng, Y.H., Kara, P. & Reid, R.C. Functional imaging with cellular resolution reveals precise micro-architecture in visual cortex. *Nature* **433**, 597–603 (2005).
30. Koulakov, A.A. & Chklovskii, D.B. Orientation preference patterns in mammalian visual cortex: a wire length minimization approach. *Neuron* **29**, 519–527 (2001).
31. Yoshimura, Y., Dantzker, J.L. & Callaway, E.M. Excitatory cortical neurons form fine-scale functional networks. *Nature* **433**, 868–873 (2005).
32. Bandyopadhyay, S., Shamma, S.A. & Kanold, P.O. Dichotomy of functional organization in the mouse auditory cortex. *Nat. Neurosci.* **13**, 361–368 (2010).
33. Rothschild, G., Nelken, I. & Mizrahi, A. Functional organization and population dynamics in the mouse primary auditory cortex. *Nat. Neurosci.* **13**, 353–360 (2010).
34. Hromádka, T., Deweese, M.R. & Zador, A.M. Sparse representation of sounds in the unanesthetized auditory cortex. *PLoS Biol.* **6**, e16 (2008).
35. Chechik, G. *et al.* Reduction of information redundancy in the ascending auditory pathway. *Neuron* **51**, 359–368 (2006).
36. Nelken, I. Processing of complex sounds in the auditory system. *Curr. Opin. Neurobiol.* **18**, 413–417 (2008).
37. Bar-Yosef, O., Rotman, Y. & Nelken, I. Responses of neurons in cat primary auditory cortex to bird chirps: effects of temporal and spectral context. *J. Neurosci.* **22**, 8619–8632 (2002).
38. Kowalski, N., Versnel, H. & Shamma, S.A. Comparison of responses in the anterior and primary auditory fields of the ferret cortex. *J. Neurophysiol.* **73**, 1513–1523 (1995).
39. Kaur, S., Rose, H.J., Lazar, R., Liang, K. & Metherate, R. Spectral integration in primary auditory cortex: laminar processing of afferent input, in vivo and in vitro. *Neuroscience* **134**, 1033–1045 (2005).
40. Metherate, R. *et al.* Spectral integration in auditory cortex: mechanisms and modulation. *Hear. Res.* **206**, 146–158 (2005).
41. Ts'o, D.Y., Gilbert, C.D. & Wiesel, T.N. Relationships between horizontal interactions and functional architecture in cat striate cortex as revealed by cross-correlation analysis. *J. Neurosci.* **6**, 1160–1170 (1986).
42. Rockland, K.S. & Lund, J.S. Widespread periodic intrinsic connections in the tree shrew visual cortex. *Science* **215**, 1532–1534 (1982).
43. Boyden, E.S., Zhang, F., Bamberg, E., Nagel, G. & Deisseroth, K. Millisecond-timescale, genetically targeted optical control of neural activity. *Nat. Neurosci.* **8**, 1263–1268 (2005).

ONLINE METHODS

Slice preparation and electrophysiology. Experiments used C57Bl6 and CBA mice and Long Evans rats under protocols approved by the Cold Spring Harbor Laboratory Animal Committee. We used young and adult mice from postnatal days 20 to 60 and juvenile rats (postnatal days 25–30). Animals were anesthetized and decapitated and the brains were transferred to a chilled cutting solution composed of (in mM) 110 choline chloride, 25 $NaHCO_3$, 25 D-glucose, 11.6 sodium ascorbate, 7 $MgCl_2$, 3.1 sodium pyruvate, 2.5 KCl, 1.25 NaH_2PO_4 and 0.5 $CaCl_2$. To examine synaptic connectivity along the tonotopic axis, we made horizontal slices with a 15° angle between the blade and the medial-lateral axis to obtain apical dendrites parallel to the slice and preserve thalamocortical axons[12]. To examine synaptic connectivity along the isofrequency axis, we made coronal slices. All slices were 300 µm thick and were transferred to artificial cerebrospinal fluid (ACSF) containing (in mM) 127 NaCl, 25 $NaHCO_3$, 25 D-glucose, 2.5 KCl, 1 $MgCl_2$, 2 $CaCl_2$ and 1.25 NaH_2PO_4, aerated with 95% O_2 5% CO_2. The slices were incubated at 34 °C for 20–30 min and then kept at room temperature (22 °C) during the experiments. We also examined thalamocortical connectivity using an auditory thalamocortical slice in the mouse (500 µm thick[12]).

Excitatory neurons 45–80 µm below the surface of the slice were visualized using infrared gradient contrast optics and patched with electrodes (6–7 MΩ) containing the following intracellular solution (in mM): 128 potassium methylsulfate, 4 $MgCl_2$, 10 HEPES, 1 EGTA, 4 Na_2-ATP, 0.4 Na_2-GTP, 10 sodium phosphocreatine and 0.015 Alexa 594 (Molecular Probes), pH 7.25; 300 mOsm. The presence of Alexa 594 in the internal solution rendered cells fluorescent. We confirmed that cells were excitatory by visualizing their dendritic arbor and spines. Filling each recorded cell with a fluorescent marker also gave us a way to reliably measure the angle between the slice and the neuronal processes to get immediate confirmation that in both horizontal and coronal slices the main arborizations were intact. Whole-cell recordings were made using a Multiclamp 700A amplifier (Axons Instruments, Molecular Devices). Excitatory currents were measured at a holding potential of −70 mV, and action potentials were recorded in cell-attached configuration.

Laser scanning photostimulation by glutamate uncaging. All LSPS hardware control and data acquisition was performed using ephus (http://www.ephus.org/). We performed LSPS as described previously[3]. Briefly, we added to the external solution (in mM) 0.37 nitroindolinyl-caged glutamate (Tocris), 0.005 3-(2-carboxypiperazin-4-yl)propyl-1-phosphonic acid (CPP, Tocris), 4 $CaCl_2$ and 4 $MgCl_2$. Focal photolysis of the caged glutamate compound was accomplished with a 1-ms light stimulus consisting of 100 pulses from a pulsed ultraviolet laser (wavelength, 355 nm with a repetition rate of 100 kHz; DPSS Lasers).

The stimulus grid for LSPS mapping in mouse cortical slices consisted of a 16 × 16 grid with 75-µm spacing, resulting in a mapping region of 1.125 × 1.125 mm. In rat cortical slices the stimulus grid was 20 × 20 with 75-µm spacing, resulting in a mapping region of 1.425 × 1.425 mm. For thalamic uncaging in auditory thalamocortical slices in the mouse, the stimulus grid was 16 × 16 with 60-µm spacing (mapping region of 900 × 900 µm). The pattern of stimulation was designed to avoid revisiting the vicinity of sites recently stimulated (see ref. 3 for details). Ultraviolet flashes were presented every 1 s. Each trial included a test pulse to measure electrophysiological parameters.

To align the stimulus grid consistently for all cells in horizontal (tonotopic) slices, we used two landmarks. We centered the *x* axis of the grid on the anterior end of the hippocampus (where the fimbria exits the hippocampus). For the *y* axis we aligned the second row of the stimulus grid to the L1–L2 border because it is the most prominent layer boundary in the auditory cortex. In the rat auditory cortex, for the *y* axis we aligned the third row of the stimulus grid on the L1–L2 border, and the center of the *x* axis on the border of CA3 and the dentate gyrus. Although we refer to low and high frequency areas in the tonotopic slice, we did not assess tonotopy for each preparation, so these are putative labels.

To align the stimulus grid consistently for all cells in coronal (isofrequency) slices, we also used two landmarks. We centered the *x* axis on the boundary between the dorsal and ventral divisions of the lateral geniculate nucleus. We centered the *y* axis in the same way as in the horizontal slices. Owing to small variations between slices in the *x*-axis alignment, we shifted the input maps so that all the somata were aligned to the center of the map in average maps. For each cell, we measured the following spatial coordinates: distance from the soma to the pial surface, to the L1–L2 border, and to the horizontal center of the map. For thalamic uncaging, the stimulus grid was placed to cover the entire MGBv.

To measure how far from the soma an ultraviolet flash can evoke an action potential and to calibrate the laser power across cells, we performed cell-attached recordings to detect action potentials from cells in L4, L5 and L6 to construct excitation profiles (**Supplementary Fig. 10**). To construct these maps, a smaller stimulus grid was used: for L4 and L6 neurons, an 8 × 8 grid with 50-µm spacing; for L5 pyramidal neurons, an 8 × 16 grid with the same spacing to test for dendritically evoked spiking. From these measurements, we found that a 30-mW laser power evoked robust and reliable synaptic responses in the cells patched while maintaining the spatial resolution of the technique (how far from the soma action potentials can be evoked) to less than 100 µm (refs. 2,5).

Analysis of LSPS data. To isolate synaptic input responses, the mean current amplitude per stimulus site was calculated in the 50 ms epoch after the direct response time window (7.5 ms after ultraviolet stimulus) and expressed as mean charge transfer (current (pA) times synaptic epoch (ms)). The values for each stimulus site are represented as pixels in a color map. For every cell, we obtained two to four maps to create an average input map. These averaged single-cell maps were used for group averages and for all analyses. Interpolated maps are used for illustration purposes only. Given the low correlation of neighboring neurons in A1, we chose to analyze laminar contributions on a single-cell basis to reduce noise. To calculate the contribution of synaptic input from each presynaptic layer on a single-cell basis, we found the pixel with the maximum value and included pixels greater than 50% of this maximum to calculate the mean. We only included perisomatic pixels that had more than 50% of the cells in the group being analyzed to avoid poor averaging due to direct stimulation sites. We also analyzed presynaptic laminar projections from average population maps (**Supplementary Fig. 11**) and found similar trends. To find the horizontal distance between the soma and the infragranular sites (pixels) with the strongest excitatory inputs (hotspot), we analyzed the portion of the input maps below L4 (**Fig. 4a**). We summed the synaptic input along columns and found the column contributing the highest input and included (as part of the hotspot) neighboring columns that were within 1 s.d. of the summed columnar input (across all columns). The distances reported are to the center of the hotspot. In this analysis, we did not include cells with input maps containing more than one hotspot.

Most laminar boundaries were determined for every slice; the markings in each figure represent the averages of the thicknesses measured. The boundary between L1 and L2 is clear from the almost complete absence of neurons in L1. Layer 2 is the densest layer in A1, and its boundary with L3 was evident upon visual inspection. Further, there were morphological and functional differences between these two layers, which we examined extensively in our study. The boundary between L3 and L4 is poorly defined in the rat and mouse A1. Both layers are populated by pyramidal cells (L4 lacks spiny stellate cells), both receive thalamic input, and in our tracing experiments we found that they both send commissural axons to the contralateral A1. Further, Nissl staining does not produce consistent cell-density differences between these layers[11]. Therefore, we relied on L3 and L4 thicknesses reported in a previous study[11]. The transition from L4 to L5 was clear from the presence of large pyramidal cells in L5. Finally, L5 and L6 differed in the shape and size of their pyramidal cells. All of our laminar boundaries are consistent with a previous study on laminar variation in the mouse auditory cortex[11].

***In vivo* recording methods.** *Surgery*: We made a craniotomy (2 mm by 3 mm) on the left auditory cortex of anesthetized (30 mg per kilogram body weight ketamine, 0.24 mg kg^{-1} medetomidine) CBA mice aged 28–35 d to perform cell-attached recordings (10–50 MΩ seal). We targeted neurons in the same area and layers characterized *in vitro* (L2/3 140–300 µm below the cortical surface) using patch electrodes containing the same intracellular solution described above, except that instead of Alexa 594 we used biocytin (1%).

Stimuli: All recordings were conducted in a double-walled sound booth (Industrial Acoustics Company). We used a custom built real-time Linux system (200 kHz sampling rate) driving a Lynx L22 audio card (Lynx Studio Technology) with an ED1 electrostatic speaker (Tucker-Davis) in free-field configuration (speaker located 8 cm lateral to, and facing, the contralateral ear). The stimuli used were 100- and 500-ms-long pure tones of 16 frequencies logarithmically spaced between 1 to 40 kHz, presented at 5, 20, 50 and 80 dB sound pressure level. All tones were

presented in a fixed pseudorandom sequence at a rate of one tone per 2 s. We also used 100-ms-long white noise stimuli presented at 20, 50 and 80 dB sound pressure level. Based on the timing and tuning properties of the single units and local field potentials (LFPs) at multiple locations, we determined that the region mapped was the primary auditory cortex[9]. To further corroborate the location of our *in vivo* recordings and to confirm that the anatomical location of our coronal and horizontal slice recordings were from the primary auditory cortex of the mouse, in some animals we combined LFP recordings with injections of a fluorescent dextran (**Supplementary Fig. 12**; tetramethylrhodamine 3,000 MW, Molecular Probes).

Histology: After physiological characterization of each neuron, we performed juxtacellular filling[17,18] and perfused mice using 4% paraformaldehyde in phosphate buffer. We unambiguously recovered 20 neurons (10 from L2 and 10 from L3).

Analysis: To quantify any changes in the firing rate during pure tones, we divided the responses to the 100-ms-long into eight 25-ms epochs, which included 50 ms before the stimulus and 50 ms after. For the 500-ms-long tones, we divided the responses into eight 100-ms epochs, which included 100 ms before the stimulus and 200 ms after. In the frequency domain, responses were grouped into half octaves. This gave us an 8 × 8 matrix of responses for each intensity. We subtracted the pre-stimulus spontaneous rate from the corresponding trials and then found the maximum response in the post-stimulus period. Finally, we took the average of the maxima for 20, 50 and 80 dB and compared these measurements between L2 and L3.

DiI retrograde tracing. To determine whether the cortical area mapped in the mouse auditory cortex was primary auditory cortex, we made small injections of DiI (dissolved in xylene to restrict spatial spread of the tracer) in thalamocortical slices. This slice preparation was developed to capture projections from the MGBv to primary auditory cortex[12]. Injected thalamocortical slices (500 μm thick) were incubated for 4–6 weeks at 37 °C ($n = 6$).

Cholera toxin injections. To characterize the laminar pattern of contralateral projections from the left auditory cortex (the hemisphere where all data was collected) to the right auditory cortex, we injected the retrograde tracer cholera toxin subunit B (Alexa Fluor 488 conjugate, Invitrogen, Molecular Probes). We performed a small craniotomy (1 mm × 1 mm) over the right auditory cortex under the same anesthesia and protocols described for the *in vivo* recordings. Using a Picospritzer (Parker Instrumentation), we injected the tracer at a concentration of 2 μg μl^{-1}; the injection site spanned all cortical layers. Mice ($n = 4$) were allowed to recover for 3 d to 1 week before being perfused.

Statistical analysis. Analysis of significant differences was performed using unpaired *t*-tests and one-way analysis of variance, with significance defined as $P < 0.05$. All data points are plotted ± s.e.m. unless otherwise noted.

doi:10.1038/nn.2659